Charge Carrier and Exciton Dynamics in Perovskites Revealed by Time-Integrated Photoluminescence after Double-Pulse Excitation

Milian Kaiser, Yang Li, Saba Gharibzadeh, Bryce S. Richards, Ulrich W. Paetzold, and Ian A. Howard*

The rate constants that describe the decays of excited states (free charge carriers, excitons) are important parameters for perovskite materials. Typically, these rates are determined using detectors with high time-resolution to record the time-dependent photoluminescence on the nanosecond scale. Herein, a method is applied that uses two excitation pulses with a variable delay and an inexpensive detector capable of measuring only the quasisteady state photoluminescence. Based on how the time-integrated photoluminescence varies as a function of the delay time between the two excitation pulses, the rate constants for exciton–exciton annihilation, monomolecular exciton decay, bimolecular free charge carrier recombination, and monomolecular trapping of free charge carriers can be extracted. To demonstrate the method quasi-2D perovskites are investigated as they are known to exhibit excited-state populations that can be exciton dominated, free charge carrier dominated, or a mixture of the two. The method leads to unique curves and accurate extracted parameters in all cases. The introduced method of determining excited-state lifetimes can be used with detectors that only have a low temporal resolution. This opens the path to the spatial mapping of excited-state dynamics using standard cameras which would be attractive for quality control of photovoltaic layers.

M. Kaiser, Y. Li, B. S. Richards, U. W. Paetzold, I. A. Howard
Institute of Microstructure Technology
Karlsruhe Institute of Technology
Hermann-von-Helmholtz-Platz 1, 76344 Eggenstein-Leopoldshafen, Germany
E-mail: ian.howard@kit.edu
Y. Li, S. Gharibzadeh, B. S. Richards, U. W. Paetzold, I. A. Howard
Light Technology Institute
Karlsruhe Institute of Technology
Engesserstrasse 13, 76131 Karlsruhe, Germany

The ORCID identification number(s) for the author(s) of this article can be found under https://doi.org/10.1002/admt.202200152.

1. Introduction

Quasi- 2D perovskite semiconductors are interesting materials for photovoltaics (PV) and perovskite light-emitting diodes (PeLEDs) due to their high stability and quantum efficiency.[1–11] PeLED devices based on these perovskites have reached external quantum efficiencies of 20% utilizing iodide[11] and 15% utilizing bromide,[10] which emit at ≈800 and 520 nm, respectively. Layered quasi-2D perovskites consist of large organic cations (2D-spacers) that separate the perovskite crystal layers and create quantum wells (QWs) of varying thicknesses. The general formula of a Ruddlesden–Popper quasi-2D perovskite is $L_2(SMX_3)_{n-1}MX_4$ where L is the 2D-spacer, S is either a monovalent metal cation or a small organic cation, M is a divalent metal cation, and X is a halide.[1,2,12–14] The parameter n represents the thickness of the 2D layers in perovskite octahedral units $[MX_6]^{4-}$. For $n = 1$, the perovskite QWs are truly 2D and the QWs can be produced in a "phase pure" manner, meaning all QWs have the same thickness.[15]

When $n > 1$, the materials are called quasi-2D perovskites and there is a variance in the QW thicknesses present in a film. These multiple-quantum-well structures (MQWs) exhibit interesting characteristics that are not present in 2D-perovskites, like energy funneling. The thickness of the QWs in an MQW affects the bandgap and exciton binding energy with thicker QWs having lower bandgaps and lower exciton binding energies due to decreased confinement.[16–20] Thin QWs have higher absorption coefficients, even when free carrier absorption dominates high above the bandgap, due to the strong Coulombic interaction between free electrons and holes.[21] Therefore, photoexcitation well above the bandgap leads to an energy transfer from thin QWs toward thick QWs, where finally radiative recombination occurs–often referred to as a funneling process.[4,5,22,23] This energy funneling allows radiative recombination to dominate trapping in the emitting QWs and increases the photoluminescence (PL) emission compared to a phase pure perovskite. High variance in QW thicknesses can decrease the emission efficiency due to large spatial and
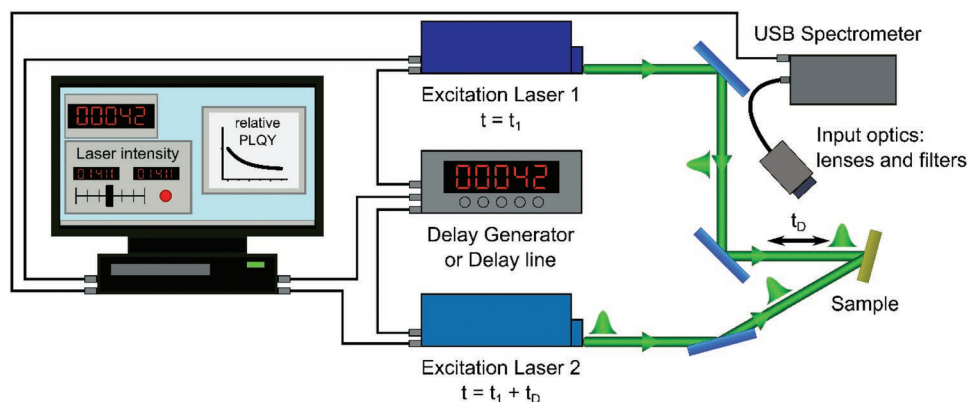
Figure 1. Experimental setup for determining the decay constants of the excited-state populations through double-pulse excitation (e.g., at 530 nm). A computer sets a digital delay generator to specify the delay between two Q-switched laser pulses (with a repetition rate of, e.g., 1 kHz). The time-integrated photoluminescence (PL) is measured of the two-pulse train with the given delay over a collection window that is long compared to the repetition rate of the lasers (i.e., the quasi-CW PL is recorded for a given pulse delay). The delay is then altered, and the PL measured for a train with a different delay between the pulses. This is repeated for a desired set of time delays. To extract the rate constants, the PL measured per excitation photon is normalized to the PL per excitation photon when only a single pulse is present and plotted as a function of the delay time.

energetic disorder.[24] Engineering of the funneling pathways increases the radiative emission of light-emitting devices based on quasi-2D perovskites.[25]

The thickness n of the QW in which the recombination occurs plays a critical role. In previous work, the current authors found that the recombination in quasi-2D perovskites can occur via either excitons, free charge carriers, or a mixture of both depending on the size of the local minimum QW into which the initial excitation is funneled.[26] The thickness (and therefore energy) of the local minima QWs vary. If this variation straddles the critical thickness above which free charge carriers are the favored excited state and below which excitons are the favored excited state, then excitons in the thinner local minima QWs contribute to the PL, as do the free carriers from the thicker QWs. In this case, the time-resolved photoluminescence (TRPL) can be described by a two-pool model based on noninteracting exciton and free charge carrier populations. The PL can stem both from the monomolecular radiative recombination of excitons and the bimolecular radiative recombination of free charge carriers.[26]

Characterizing the nature of the excited-state populations (excitons vs free-charges) and the rates of decay from these excited states is of fundamental importance for understanding the material performance in a device setting. Although especially relevant in the quasi-2D materials due to the possibility for excitons, free charge carriers, or both to play a role in the excited-state dynamics (as introduced above), the characterization of the recombination rates of the photoexcited free-carrier population in 3D materials is also important for assessing the quality and potential performance of a given layer in a device setting. Time resolving the PL after impulsive excitation at varying fluences is an established and effective way of characterizing these rates.[26] However, this method relies on expensive and sensitive hardware, such as a streak camera or a time-correlated single photon counting apparatus, which would complicate its implementation for the in-line characterization of excited-state dynamics as a standard part of a device fabrication line.

In this contribution, we demonstrate how the excited-state dynamics of perovskites can be determined from the measurement of the time-integrated PL (TIPL) after impulsive excitation from two short optical pulses, whose intensities are controlled as is the wait time between pulses. Such an approach has already been used in the analysis of excited-state dynamics in titanyl phthalocyanine films,[27] as well as in the study of graphene layers on timescales of femto- and picoseconds[28,29] and in the analysis of the emission of nanowire lasing.[30] The setup uses a simple USB spectrometer to record the PL, and pulse sequences can be generated with Q-switched lasers (see **Figure 1**). We show that the TIPL varies as the delay between the pulses is swept. These variations with pulse delay are different for exciton and free-carrier populations. The TIPL decreases with decreasing delay between the pulses for exciton populations, as exciton–exciton annihilation increases and thereby decreases the net photoluminescence quantum yield (PLQY). While we do not absolutely measure the PLQY we observe the relative change in the PLQY via the change in the PL emission which depends on the PLQY. On the other hand, for the free charge carrier population, the TIPL increases with decreasing separation between the optical pulses as higher charge-carrier densities lead to faster bimolecular radiative recombination and a higher net PLQY and thereby stronger emission (due to better competition of the bimolecular radiative rate with the monomolecular nonradiative trapping rate). Furthermore, it is shown that the rate constants for exciton–exciton annihilation, monomolecular exciton decay, bimolecular free charge carrier recombination, and monomolecular trapping of free charge carriers can be extracted from an analysis of the PLQY of the double-pulse sequence relative to a single pulse as a function of the time delay between the pulses. Finally, the potential advantages of this new method in terms of allowing in-line or even "imaging" of the excited-state rate constants with robust detectors in a production setting are discussed.

2. Results and Discussion

The following presents how the key rates describing the excited-state dynamics in a perovskite layer can be extracted

**ADVANCED
SCIENCE NEWS**
www.advancedsciencenews.com

**ADVANCED
MATERIALS
TECHNOLOGIES**
www.advmattechnol.de

by measuring the TIPL under a sequence of double pulses if the pulse intensities and their relative delay can be controlled. In Section 1, we extend a previously presented model to simulate how the TIPL varies with changing delay between pulses, demonstrate how the qualitative features of the variance of the TIPL reveal the nature of the excited-state species present and show how the relative PLQY as a function of interpulse delay can be fit to uniquely determine the relevant rate constants. In Section 2, we apply the method and analysis to the test case of quasi-2D perovskite films wherein the excited state population can be varied (by adjusting the type and concentration of the 2D spacer) to give a pure exciton population, a pure free charge carrier population, or a mixture of the two. We show that in all these cases the method and model can characterize and extract the various photophysical rates.

2.1. Simulation

2.1.1. Excitonic Photoluminescence

In a perovskite wherein excitons are the only excited state, the temporal change in exciton density can be described as

$$\frac{dn_x}{dt} = -k_x n_x - \gamma_{EEA} n_x^2 \tag{1}$$

where n_x is the exciton density, k_x is the monomolecular exciton recombination rate constant (consisting of both the radiative recombination and nonradiative pathways) and γ_{EEA} is the exciton–exciton annihilation (EEA) rate (leading to the nonradiative decay of a single exciton). From this equation, we can see that at low exciton densities the EEA plays a lesser role, and most excitons recombine via the monomolecular rate. The opposite is true for high exciton densities. As EEA is an additional nonradiative loss, the PL emission must decrease as the fluence is increased, and thereby the exciton density

increases—see Figure S1 in the Supporting Information for a simple example of how the PLQY and thereby emission changes with the initial exciton density under pulsed excitation. For the double-pulse experiments, the implication of the PL emission being lower at higher exciton densities is that at short temporal delays between the two pulse trains the TIPL will be lower than that at longer delays. To analyze the changes in PL emission at a specific delay, we introduce the relative PLQY which we get by dividing the TIPL at a set time delay by twice the TIPL for a train of single pulses given that both pulses have the same fluence. This is described in **Figure 2**a, where the PL intensity as a function of time is shown for a single pulse and double pulses at a "short" time delay. The experimentally observed TIPL is directly proportional to the integrals under these curves. The relative PLQY obtained by dividing the TIPL observed with the double-pulse train by twice that observed in a reference measurement with a single pulse train (one of the lasers blocked) goes to unity at long delays and drops below unity once the delays become short enough that a significant exciton population from the first pulse is still present when the second pulse arrives. This is shown in Figure 2b, where N_0 is the initial density of excitons generated by an excitation pulse. For the simulations in Figure 2b, the rate constants are based on our experimental results below and are: $k_x = 30 \times 10^7$ s^{-1}; $\gamma_{EEA} = 1 \times 10^{-10}$ cm^3 s^{-1}. The functions used to simulate the relative PLQY as a function of delay are detailed in Supporting Information, as is their derivation.

The area under the curves in Figure 2a represents the TIPL. For short time delays between the pulses, the residual population from the first pulse at the time of arrival of the second pulse is significant. This pushes the excited-state density higher than the maximum reached by a single pulse alone and has the consequence that more excited states are lost to EEA. The integral under the curve corresponds to the experimentally observed TIPL and is shown in gray for the double-pulse excitation and red for the reference single pulse experiment (wherein one laser is simply blocked). Dividing the gray area by twice the red
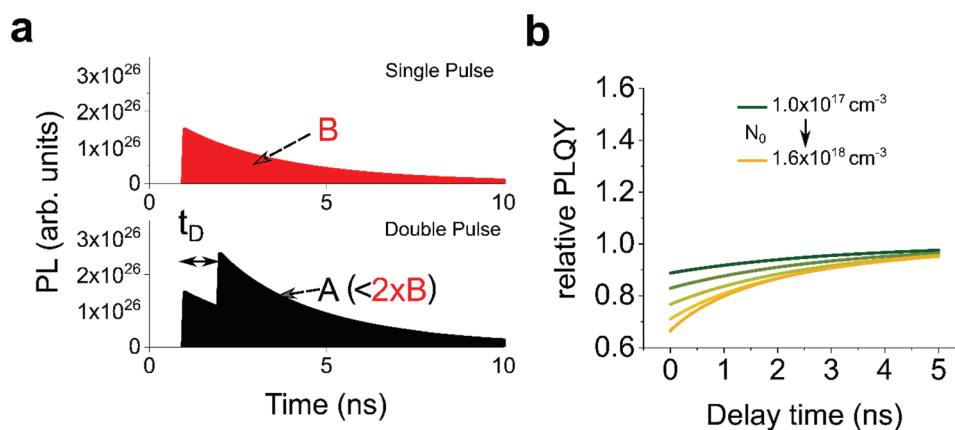

Figure 2. a) Simulation of the time-dependent exciton PL of a single and a double-pulse excitation wherein both pulses generate the same initial density ($N_0 = 5 \times 10^{17}$ cm^{-3}). For a "short" delay t_D (1 ns, bottom) the residual exciton population from the first pulse pushes the total exciton population after the second pulse to higher values and thus decreases the PLQY relative to the PLQY of a single pulse (top) due to increased exciton-exciton annihilation. b) the relative PLQY can be defined as the number of photons observed per total excitation photons in the double-pulse normalized to the number of PL photons per excitation photon for a single pulse only. At long time delays, the relative PLQY approaches the limit of unity. For additional information, the curves are shown for changing pulse fluence (the exciton density created by a single pulse is carried from 10^{17} to 1.6×10^{18} cm^{-3}).

**ADVANCED
SCIENCE NEWS**
www.advancedsciencenews.com

**ADVANCED
MATERIALS
TECHNOLOGIES**
www.advmattechnol.de

area gives the relative PLQY for a given time delay. This relative PLQY as a function of time delay is presented in Figure 2b. We note that the delay time is the relative delay between the two pulses, and if this could be arbitrarily controlled so that the second pulse could not only be brought to be concurrent with the first pulse (0 delay) but also to precede the first pulse (a negative delay), then the same trend in relative PLQY as measured for positive delay times would also be measured for negative delay times (the curve shown in Figure 2b would be mirrored about 0 delay time). Also, the different curves for changing the fluence of both pulses are shown, the exciton density created by an individual pulse is varied from 10^{17} to 1.6×10^{18} cm^{-3}. For short time delays, the relative PLQY is the lowest due to EEA being the most dominant in this region. As the delay between the pulse trains increases the relative PLQY increases towards unity. The relative PLQY curve as a function of delay time shown in Figure 2b contains sufficient information to extract the rate constants. Of course, a simple steady-state PLQY measurement on its own does not contain enough information to determine rates. A Gedankenexperiment to demonstrate this: if both rate constants were to increase by an order of magnitude, then the PLQY would not change. However, such an increase in rate constants would change the relative PLQY curve, it would move toward unity at much shorter delays. At a given initial excitation density the relative PLQY curves for all combinations of rate constants are unique. The uniqueness of the curves and thereby the ability to extract unique and accurate parameters is shown in the Supporting Information by simulating noisy data and fitting it at different initializations (refer to Figure S2, Supporting Information). So, by measuring and fitting an experimental curve at a single fluence it is possible to accurately extract the rate constants. We note however that the excitation densities must be high enough for EEA to occur. At too low excitation densities the relative PLQY would always be the same as EEA never makes a significant difference to the exciton density.

2.1.2. Free Charge Carrier Photoluminescence

When the excited-state population is comprised of free charge carriers rather than excitons the behavior under the double-pulse experiment is very different. For free charge carriers, the monomolecular process is associated with nonradiative loss (due to carrier trapping), whereas the bimolecular rate is associated with radiative recombination. This is precisely opposite to the case for an excitonic excited population. For the free charge carriers, the rate equation describing the population dynamics has an analogous form

$$\frac{dn_c}{dt} = -k_{1,c}n_c - k_{2,c}n_c^2 \tag{2}$$

Here n_c is the carrier density, $k_{1,c}$ is the free charge carrier trapping rate constant associated with nonradiative decay, and $k_{2,c}$ is the bimolecular radiative recombination rate constant. Switching of the monomolecular term being the nonradiative rate and the bimolecular term being the radiative one means that the PLQY as a function of carrier density behaves oppositely to the excitonic case. For free charge carriers, at low

excited state densities most of the free charge carriers are lost via the monomolecular trapping (to thereafter decay nonradiatively) and therefore the PLQY is low. For higher excitation densities the radiative recombination competes better with the monomolecular loss and the PLQY increases. This increase in PLQY continues with the excitation intensity until at some point the nonradiative third-order process of Auger recombination begins to become significant. We show an example of how the PLQY after pulsed excitation changes as a function of the initial carrier density in a regime before Auger recombination must be considered in Figure S3 (Supporting Information). This implies double-pulse excitation at short temporal delays between the pulses, wherein the excited-state density gets pushed higher due to the residual population from the first pulse when the second pulse arrives, the PLQY is higher than for longer delays. Like with excitons we get the relative PLQY by dividing the TIPL at a set delay with twice the TIPL of the single pulse excitation. For long delays, the relative PLQY must again approach unity (the same as in the exciton case), since the pulses do not interact. However, opposite to the exciton case, the PLQY will exceed unity at shorter delays as the relative PLQY must be higher than unity, and due to the bimolecular radiative behavior, when the pulses are both the same fluence the relative PLQY cannot be higher than two. This principle is shown in **Figure 3**. The used rate constants for this simulation are based on our previous work[26]: $k_{1,c} = 70 \times 10^7$ s^{-1} and $k_{2,c} = 5 \times 10^{-10}$ cm^3 s^{-1}.

In Figure 3a, we show the simulated time-dependent PL when the excited-state population consists of free charge carriers. The derivation of the equations for simulating this behavior can again be found in the Supporting Information. In contrast to the excitonic PL, the PL becomes much stronger rather than weaker when the second pulse arrives after a short temporal delay. The relative PLQY as a function of interpulse delay is shown in Figure 3b. A distinctly different behavior than for the excitonic case is immediately apparent. The relative PLQY is above unity at short delays and moves toward unity as the delay increases. Also, interesting to note here is that as the initial densities increase (and the PLQY from an individual pulse increases) the relative PLQY increase at short times decreases. This is due to the bimolecular recombination already becoming the dominant pathway after a single pulse i.e., the increase in carrier density due to the overlap of populations from the first and second pulse leads only to a minor increase in the PLQY. Like with excitons every single curve is unique and the rates can be extracted by fitting a single curve with a known initial free carrier density (see Figure S4, Supporting Information). Here, we note that at exceedingly high excitation densities the relative PLQY does not change with the time delay, or that the change will be influenced by Auger recombination. To best observe the relative PLQY curve an excitation fluence should be chosen that is high enough that the PL is observable with a good signal to noise ratio, but low enough that the bimolecular rate does not dominate at the densities created by a single pulse (and therefore also Auger effects can be neglected). A practical rule of thumb will be presented below that the excitation fluence should be chosen such that initial decay due to trapping and bimolecular recombination are equal. This condition gives a good compromise between a large change in relative PLQY occurring as a function of delay time, and also the PL signal being large enough to be easily measured.
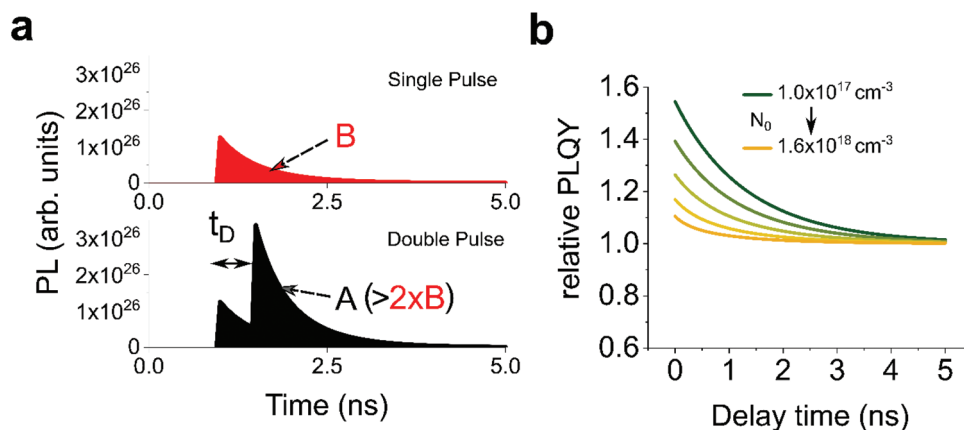
**ADVANCED
SCIENCE NEWS**
www.advancedsciencenews.com

**ADVANCED
MATERIALS
TECHNOLOGIES**
www.advmattechnol.de

Figure 3. a) Simulation of the time-dependent free carrier PL of a single and a double-pulse excitation wherein both pulses generate the same initial density ($N_0 = 5 \times 10^{17}$ cm^{-3}). For a "short" delay t_D (0.5 ns, bottom) the residual free carrier population from the first pulse pushes the total free carrier population after the second pulse to higher values and thus increases the PLQY relative to the PLQY of a single pulse (top) due to increased bimolecular radiative recombination. b) The relative PLQY can be defined as the number of photons observed per total excitation photons in the double-pulse normalized to the number of PL photons per excitation photon for a single pulse only. At long time delays, the relative PLQY approaches the limit of unity. For additional information, the curves are shown for changing pulse fluence (the free carrier density created by a single pulse is carried from 10^{17} to 1.6×10^{18} cm^{-3}).

2.1.3. Exciton and Free Charge Carrier Photoluminescence

We have found previously that some quasi-2D perovskites can support both independent excited-state population pools of excitons and free charge carriers.[31–34] In this (albeit specialized) case, a linear combination of the two models above can be used to simulate the behavior. Different perovskites showing similar behavior might also be analyzed with the introduced method. We will demonstrate this below for experimental data on these specific quasi-2D films to show that even in this case the double-pulse method gives unique data that support previous analysis. For most perovskite films, either the excitonic model or the free charge carrier model alone should be sufficient (with the latter being the most appropriate for the standard 3D films).

3. Experimental Data

To demonstrate the double-pulse technique, we analyze a variety of quasi-2D perovskite materials the photophysical behavior of which we are already familiar with. In previous work, we found that the amplified spontaneous emission (ASE) thresholds of quasi-2D perovskites depended on the 2D spacer molecule used, and its concentration in the perovskite precursor.[33] Following this up, we established that the type of 2D spacer and its concentration could tune the dominant excited-state species from excitons to free charge carriers, and even in specific conditions lead to a noninteracting mixture of excitons and free charge carriers.[26] The access to all of these excited state species makes this series an ideal test of the double-pulse technique as illustrated below.

The quasi-2D perovskite samples used in this work were fabricated by adding either butylamine bromide (BABr) or 1-naphthylmethylamine bromide (NMABr) spacer molecules to CsPbBr$_3$ dissolved in Dimethyl sulfoxide (DMSO) to reach an elemental composition of CsPbBr$_3$(BABr)$_y$. The fabrication method is further explained below. In our previous work,[26] we found that using high concentrations of BA leads the excited state population to entirely consist of excitons while at lower BA concentrations noninteracting populations of both excitons and free charge carriers are supported in different local energy minimum QWs. Using NMA as the 2D spacer on the other hand leads the excited-state population to comprise only free charge carriers.[26] This is consistent with previous work on Dion–Jacobson perovskites using p-xylylenediamine spacers.[35] In this section, we show that the double-pulse technique works to extract the key kinetic parameters from the experimental data when the excited state population is dominated by excitons or free charge carriers, and even in the oddly complicated case that concurrent noninteracting populations of the two coexist. In this sense, we show the general applicability of this technique for perovskite materials (either 2D, quasi-2D, or 3D).

For our perovskites, the excited-state lifetimes are short, on the scale of fewer than 10 ns. This led us to use a delay stage rather than a delay generator (as depicted in Figure 1) to control the delay more precisely between pulses. For 3D materials which have slower monomolecular rates, a delay generator would be sufficient.

For the relative PLQY, we divide our TIPL curves after double-pulse excitation by twice the TIPL of a single pulse excitation. Both excitation pulses are set to the same fluence. The repetition rate was 1 kHz for the NMA spacer perovskites and 100 Hz for the BA spacer perovskites. Thus, the repetition rates are sufficiently low that all excited-states created by a given pulse pair have recombined before the next pulse pair arrives 1 ms (or more) later.[36] The integration time on the CCD was 80 ms and ten averages were taken to measure the TIPL in the quasi-steady state. The master equation used to fit the data below is shown in as Equation (S17) (Supporting Information), and the Origin fitting function used to fit the data below is also available as part of the Supporting Information.

**ADVANCED
SCIENCE NEWS**

www.advancedsciencenews.com

**ADVANCED
MATERIALS
TECHNOLOGIES**

www.advmattechnol.de

3.1. Exciton Excited State Population

We see a clear difference between the NMA and BA spacers which is in full agreement with the above and previous work on their different excited-state populations[26] (an overview Figure showing all double-pulse data next to one another to qualitatively compare is shown in Figure S5, Supporting Information). In analogy with the simulation section above, we will first examine the sample in which excitons dominate the excited-state population, namely the BA spacer at high concentration $BA_{1.0}$. The generalized fitting function is shown as Equation (S17) in the Supporting Information. This contains a parameter, f, for the fraction of the emitting QWs that support excitonic emission (with the remainder, $1 - f$, being the fraction of QWs that support free charge carrier emission). Based on our previous knowledge we will hold f to be 100% first in this case and examine the relative PLQY as a function of inter-pulse delay time for a variety of fluences. The data are depicted in **Figure 4**.

The relative PLQY as a function of the delay time demonstrates strong similarities to the simulations above. The higher the density created by the pulses and the lower the time delay, the lower the relative PLQY. As the time delay between the pulses lengthens, the relative PLQY moves back to unity. These data can be fit well when the fraction of the excited state population in the exciton pool is considered to be 100%. The fits are shown in red in Figure 4, and the mean of the extracted parameters from the two curves are $k_x = (33 \pm 2) \times 10^7$ s^{-1} and $\gamma_{EEA} = (0.80 \pm 0.1) \times 10^{-10}$ cm^3 s^{-1} with statistical errors. Further information about the fitting process is given in the Statistics section. We discuss the quality of this fit compared with a fit resulting from f being a free parameter in Figure S6 (Supporting Information). The value for k_{1x} that we extract here is faster than that we have observed for more optimized BA quasi-2D
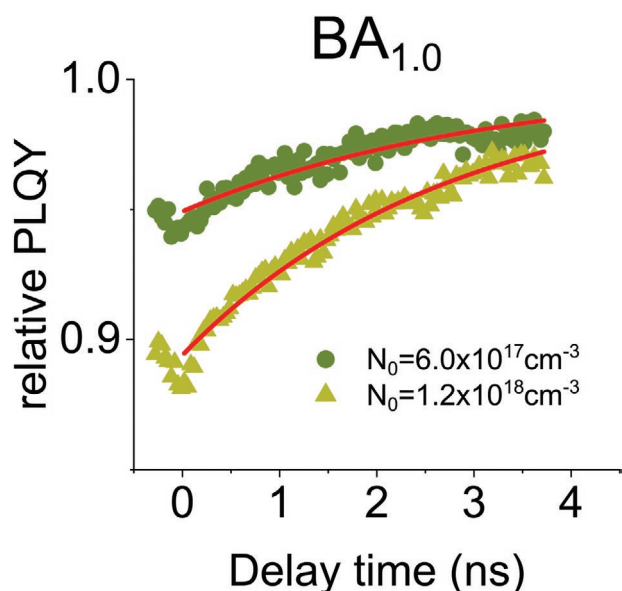
samples, which we attribute to batch-to-batch variation in film quality and high nonradiative rates in the current batches. Irrespective of this variation in material quality, the results clearly show (both qualitatively and quantitatively) that the double-pulse method works well for experimental data wherein the excited-state population is dominated by excitons.

3.2. Free Charge Carrier Excited State Population

The excited-state population in quasi-2D perovskites based on NMA spacers was found to be dominated by free charge carriers[26,33] and therefore we choose to use $NMA_{1.0}$ to check the double-pulse method for experimental data wherein the excited state population is dominated by free charge carriers. The domination of free charge carriers for this sample can be qualitatively confirmed by comparing the data for $NMA_{1.0}$ shown in **Figure 5** below with that shown for the exciton-based $BA_{1.0}$ shown above. In contrast to the exciton dominated BA, for the free charge carrier dominated $NMA_{1.0}$ the relative PLQY starts well *above* unity at short delay times between the pulses, and its offset from unity *decreases* with increasing fluence. This significantly different qualitative behavior is as expected for perovskite materials whose excited-state populations are dominated by excitons versus free charge carriers and demonstrates the utility of this technique in terms of obvious qualitative differences in the measured data revealing the dominant excited-state species.

To fit these data, we follow an analogous procedure to the above. If we first constrain the fraction of the exciton population to be 0%, the fits shown in red in Figure 5 are obtained, and the parameters $k_{1,c} = (38 \pm 6) \times 10^7$ s^{-1} and $k_{2,c} = (14 \pm 2) \times 10^{-10}$ cm^3 s^{-1} are extracted. The quality of the fit does not become better if the fraction of excitons is left as a fitting parameter, this is discussed in Figure S7 (Supporting Information). These
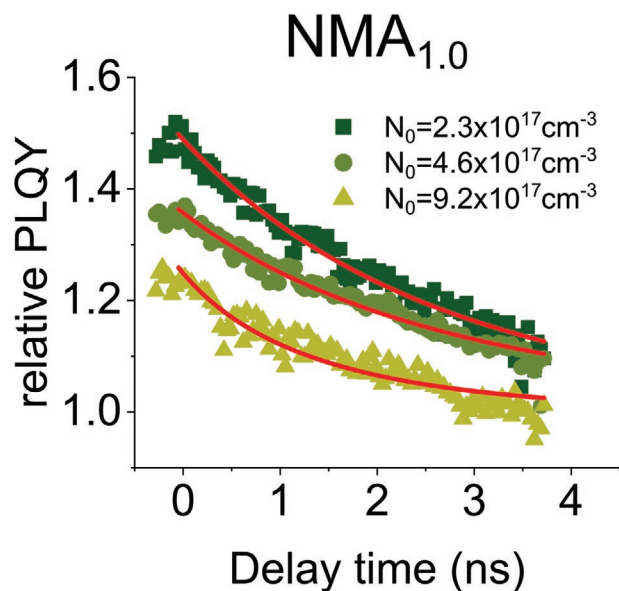

Figure 4. Relative PLQY over the time delay between the two excitation pulses for the $BA_{1.0}$ perovskite at different excitation fluences. The extracted parameters are $k_x = (33 \pm 2) \times 10^7$ s^{-1} and $\gamma_{EEA} = (0.80 \pm 0.1) \times 10^{-10}$ cm^3 s^{-1}.

Figure 5. Relative PLQY over the time delay between the two excitation pulses for the $NMA_{1.0}$ perovskite. The extracted parameters are $k_{1,c} = (38 \pm 6) \times 10^7$ s^{-1} and $k_{2,c} = (14 \pm 2) \times 10^{-10}$ cm^3 s^{-1}.

ADVANCED
SCIENCE NEWS

www.advancedsciencenews.com

ADVANCED
MATERIALS
TECHNOLOGIES

www.advmattechnol.de

values are well within an order of magnitude agreement with those previously determined, with the differences being attributed to the considerable influence of sample preparation in these highly disordered quasi-2D perovskites. Nonetheless, these data again clearly demonstrate how qualitatively and quantitively the dynamics of a free charge carrier-dominated excited-state population can be extracted by the double-pulse technique.

3.3. Excitons and Free Charge Carrier Excited State Populations

For the final experimental test case, we examine the unique situation that we have observed in quasi-2D perovskites using lower concentrations of BA as the 2D spacer in which independent pools of coexisting excitons and free charge carriers make up the excited state population.[26] This special case shows that even complex systems of excited species can be analyzed with a simple experimental setup. The exciton and free charge carrier populations are separated in different local energy minima QWs and therefore do not interact. For this reason, the total response of the sample can be treated as the weighted sum of two independent samples, one that shows solely exciton dynamics and another that shows only free charge carrier dynamics.

The data for $BA_{0.4}$ is shown in **Figure 6**. The data exhibit a strong similarity to the entirely exciton-dominated case of $BA_{1.0}$, shown in Figure 4. The relative PLQY has a minimum at zero delay time between the pulses and approaches unity as the delay increases. This is consistent with excitons forming a sizeable portion of the total excited state population. However, there is also subtle qualitative information that is not consistent with the excited state population being entirely made up of excitons. At the lower fluence, the relative PLQY is only minorly reduced

at zero time. We would then expect a significant additional reduction in PLQY when the fluence is increased. However, this is not observed. When the fluence is doubled, the relative PLQY at zero delay time between the pulses hardly decreases (compare this to the much more significant decrease observed in Figure 4). Also, the two curves cross, with the higher fluence curve starting at a lower relative PLQY at short time delays and then crossing the lower fluence curve to have a slightly higher relative PLQY at a long-time delay.

The fit to these data is plotted in Figure 6. There are too many parameters to fit the curves individually with reasonable uncertainties for the mixed case. Instead, a global fit is used where the parameters are shared to determine the rate constants. In this case, constraining the excited-state population to be entirely free charge carriers will not work. The relative PLQY never exceeds unity and increases with increasing delay time. Likewise, constraining the excited-state population to consist entirely of excitons leads to a fit of only moderate quality (see Figure S8, Supporting Information). The fit quality is significantly enhanced, and the two qualitative features mentioned above are reproduced when a mix of noninteracting exciton and charge populations are considered. In this case, the extracted parameters are: $k_{1,c} = (24 \pm 2) \times 10^7$ s^{-1}; $k_{2,c} = (3.0 \pm 0.5) \times 10^{-10}$ cm^3 s^{-1}; $k_x = (39 \pm 2) \times 10^7$ s^{-1}; $\gamma_{EEA} = (4.8 \pm 0.4) \times 10^{-10}$ cm^3 s^{-1}; and $f = (70.3 \pm 0.3)\%$. We note here that unlike in previous fits, these uncertainties are not based on the statistical error but result from the global fit and are underestimating the real uncertainties. In the special case of simultaneous emission from both species, a fluence-dependent measurement is advisable. The fitting depends on the ratio of the radiative and nonradiative monomolecular exciton recombination as shown in Equation (S17) (Supporting Information). This ratio and the fraction of exciton-dominated QWs f are directly dependent, while all other parameters are unaffected were this ratio to be changed. For simplicity, we assume that all monomolecular exciton recombination is radiative and therefore underestimate the fraction f. The extracted parameters for the excitonic recombination are an order of magnitude higher than our previously found parameters which we ascribe to batch-to-batch variations in film quality. The parameters for free carriers however are similar to the ones extracted in our previous work as is the fraction f.[26] The double excitation pulse method therefore not only allows the extraction of rate constants for purely free carrier or exciton dominated PL emission but also for the unusual case of both excited species emitting PL.

As an additional note for the interested reader, our conclusion that a mixed population of both free charge carriers and excitons is found in the $BA_{0.4}$ sample, but none of the other samples can be supported by carefully considering the normalized PL spectrum of the samples as a function of fluence. These data are illustrated in Figure S9 (Supporting Information). For the $BA_{1.0}$ and $NMA_{1.0}$ samples, the normalized PL spectra do not change as a function of fluence. This is expected, as a single excited state dominates the excited-state population in both cases. The shape of the PL peak due to the exciton population at 2.43 eV for the $BA_{1.0}$ remains unchanged as a function of excitation fluence. So does the PL peak at 2.36 eV due to free charge carrier recombination in $NMA_{1.0}$. The fact that neither of these PL peak shapes changes with fluence is to be expected as only a
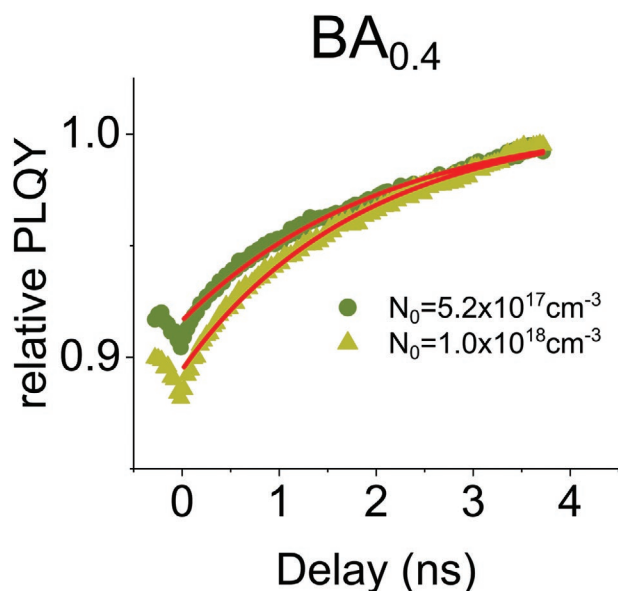

Figure 6. Relative PLQY over the time delay between the two excitation pulses for the $BA_{0.4}$ perovskite. The extracted parameters are $k_{1,c} = (24 \pm 2) \times 10^7$ s^{-1}; $k_{2,c} = (3.0 \pm 0.5) \times 10^{-10}$ cm^3 s^{-1}; $k_x = (39 \pm 2) \times 10^7$ s^{-1}; $\gamma_{EEA} = (4.8 \pm 0.4) \times 10^{-10}$ cm^3 s^{-1} and $f = (70.3 \pm 0.3)\%$.

**ADVANCED
SCIENCE NEWS**

www.advancedsciencenews.com

**ADVANCED
MATERIALS
TECHNOLOGIES**

www.advmattechnol.de

single excited-state population is responsible for the PL in each case. However, in the $BA_{0.4}$ sample where both excitons and free charge carriers contribute to the PL one would expect the shape of the PL spectrum to change with fluence as free carrier emission should contribute more significantly to the overall PL (and exciton emission less significantly) as the excitation fluence is increased. This is because at the higher excited-state density free charge carrier emission will become more efficient, and exciton emission (due to EEA) can become less efficient. Indeed, the data shown in Figure S9 (Supporting Information) support this, with the lower energy shoulder becoming increasingly visible at higher excitation fluences. The position of the lower energy shoulder is also consistent with that of the free charge carrier emission observed in NMA sample. Therefore, we note that the behavior of the PL spectra as a function of fluence also supports our above analysis concluding that while only excitons or free charge carriers dominate the excited-state populations in $BA_{1.0}$ and $NMA_{1.0}$ samples respectively, a mixture of both these populations is present in the $BA_{0.4}$ case.

3.4. Application to 3D Perovskite Photovoltaic Layers

Having established that quasi-2D perovskites with somewhat uncommon excited state dynamics can be characterized with the double pulse method, we highlight the application in 3D-perovskite materials and discuss how the significantly slower kinetics in 3D materials should allow in-line characterization of charge carrier dynamics in photovoltaic layers with the double pulse method using significantly cheaper sources (potentially LEDs). As an exemplary material, we use $Cs_{0.18}FA_{0.82}PbI_3$, with and without a passivation layer based on adding phenethylammonium chloride (PEACl) to the perovskite precursor, which forms heterogeneous 2D Ruddlesden–Popper (RP) $(PEA)_2(Cs_{1-x}FA_x)_{n-1}Pb_n(I_{1-y}Cl_y)_{3n+1}$ layers where $n \approx 1–2$ at the grain boundaries and the surface of the film. This passivation material has recently been used to fabricate MA-free solar cells with power conversion efficiencies exceeding 22%.[37] As the k_1 is much lower for 3D materials than the quasi-2D materials discussed above, significantly longer delays (and lower pulse fluences) are needed for the double pulse experiment. Therefore, instead of splitting the beam and utilizing a delay stage, a digital delay generator is used to introduce a 0.6 ns pulse from an actively Q-switched laser at a widely variable delay from the amplifier pulse. For comparison, the TRPL is taken with a streak camera after exciting the samples with the Q-switched at various fluences and the charge dynamics are also determined by the more common method of globally fitting these dynamics. We note that an exciton population need not be considered for these 3D perovskites, and the behavior for an excited state population purely made of charges is followed.

The TRPL and double pulse data for the passivated and unpassivated samples are shown in **Figure 7**. To obtain a better estimate of the uncertainty in the extracted parameters, the fluence series for each sample was remeasured three times. All measurements were performed in air. Figure 7 shows the mean and standard deviation of each data point from the three repeat measurements. To estimate the parameter values and uncertainties, each of the nine data sets was fit individually (that

is each of the three fluences for every one of the three repeat measurements was fit alone). In Figure 7, the red lines show the curves for the mean value of the parameters so extracted. The parameters and their uncertainties are summarized in **Table 1**.

We note from Figure 7 and Table 1 that the uncertainty in the unpassivated measurement and the associated extracted parameters is higher, and we attribute this to greater instability in this sample under prolonged light exposure (see Figure S10 (Supporting Information) for the systematic evolution of the curves with repeat measurements showing a light soaking like effect for the unpassivated sample but no change upon repeat measurement of the more stable passivated sample). Our current purpose is to estimate the uncertainty in extracted parameters that might be achievable in an inline monitoring system where the total exposure to light may not be that rigorously controlled. Therefore, we consider this systematic error due to light-induced change as a reasonable estimate of the random error that might occur in an inline system wherein the total light exposure is poorly controlled. This leads to a relative uncertainty in the extracted parameters of around 40% for the unpassivated sample (the relative uncertainty being similar for the TRPL and double pulse methods), whereas in the more stable passivated samples the relative uncertainty is less than 25%. Hence, we estimate that a parameter error of 25% should be achievable inline if systematic errors (such as light exposure and ambient conditions) are well controlled. Of crucial relevance to this work, the relative uncertainty in the double pulse method is equivalent to the relative uncertainty of the standard TRPL method, and the parameters extracted from both methods agree within their uncertainties.

In terms of analyzing the extracted parameters, $k_{1,c}$, is significantly decreased by the passivation. This is expected, as the purpose of passivation is the reduction of the traps at the interfaces and grain boundaries.[37] Both methods also suggest that there might be only a slight decrease in $k_{2,c}$ upon passivation. Again, this makes sense as one would not expect the carrier transport inside or between the grains to be majorly affected by this optimal passivation protocol which maintains high photovoltaic performance. In this sense, these results give a good indication that the double pulse method could be useful for inline inspection of solar cells giving a rough prediction of their carrier dynamics.

Furthermore, the above results help to guide the consideration of what light sources are necessary to perform these double-pulse experiments in-line on perovskite solar cells. We can understand the rules of thumb for the selection of pulse length and excitation fluence. To first consider fluence, for determining free charge carrier dynamics there is no theoretical lower bound for the pulse fluence. The change in relative PLQY is largest for low energy pulses (as the amount of emission always increases quadratically with the charge density in this low-density limit). However, there is a practical limitation in the pulse fluence in that it should be large enough that the photoluminescence is easily (and accurately detectable). To reach an optimum compromise between the desired large change in relative PLQY (favoring lower fluences—see Figure 7b and for experimental evidence of this) and the desired bright, easily measurable PL (favoring higher fluences) we suggest that pulse
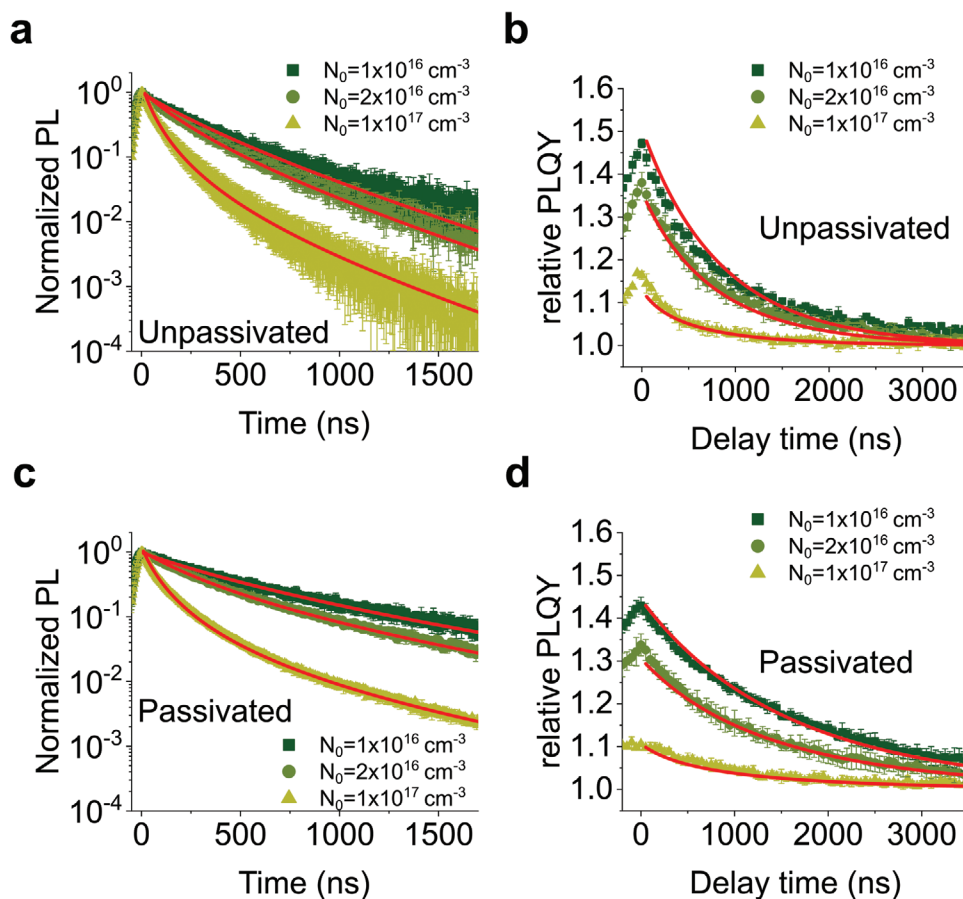
**ADVANCED
SCIENCE NEWS**
www.advancedsciencenews.com

**ADVANCED
MATERIALS
TECHNOLOGIES**
www.advmattechnol.de

Figure 7. Comparison of the rates extracted from TRPL measurements utilizing a streak camera and from the relative PLQY for an unpassivated sample a,b) and a passivated sample c,d). A single passivated and an unpassivated sample are used. The measurement method is swapped after each series of measurements of three fluences. This whole procedure is repeated three times to get three measurements for each method for each fluence. The nine data sets per sample are individually fit giving nine estimates of the extracted parameters from which the mean and uncertainty for each parameter can be estimated. These are shown in Table 1. The data shown represent the mean and standard deviation at each point based on the three separate measurements for each fluence.

fluences are used at which the rates of trapping and bimolecular recombination are equal at zero time. Explicitly, an excitation fluence is chosen so that $k_{1,c} \approx k_{2,c}N_0$. The two lower fluences in Figure 7b,d correspond to this condition, with $k_{1,c} \approx 1 \times 10^6$ s^{-1} $\approx 1 \times 10^{-10}$ cm^3 s^{-1} $\cdot$ 1×10^{16} cm^3 $\approx k_{2,c}N_0$. In this case, the relative PLQY is ≈ 1.5 at zero time, so there is a substantial enough change in relative PLQY that the data can be easily fit, and the emission is strong enough that it is easily collected. Now so that the excitation can be approximated as impulsive for the fitting we consider that the excitation pulse should be 5 times shorter than the inverse of the total decay rate at zero time. For the condition established as a rule of thumb above,

the total decay rate at zero time is simply $2 \cdot k_{1,c}$, which for good photovoltaic materials such as those above should be around 2×10^6 s^{-1}. Thus, a pulse as long as 100 ns could still be considered impulsive in this case. Obtaining 100 ns pulses with a pulse fluence on the order of 1 µJ from arrays of LEDs is possible,[38] and a 1 µJ pulse energy is sufficient to create a charge carrier density around 10^{16} cm^{-3} over a circular area of ≈ 1 mm radius in a 100 nm thick perovskite film. Also, developments of LED systems for Li-Fi could be exploited here to obtain the desired pulse sequences.[39] Therefore, these back of envelope calculations based on the above results establish that lower-cost systems based on pulsed LEDs with a controllable

Table 1. Fitting parameters obtained from the fits shown in Figure 7. Uncertainties quoted are those from the fitting algorithm.

Method	$k_{1,c}$ [s^{-1}]		$k_{2,c}$ [cm^3 s^{-1}]	
	Unpassivated	Passivated	Unpassivated	Passivated
TRPL	$(1.1 \pm 0.4) \times 10^6$	$(0.43 \pm 0.09) \times 10^6$	$(10 \pm 4) \times 10^{-11}$	$(8 \pm 1) \times 10^{-11}$
Double Pulse	$(1.0 \pm 0.4) \times 10^6$	$(0.6 \pm 0.1) \times 10^6$ s^{-1}	$(9 \pm 2) \times 10^{-11}$	$(6 \pm 1) \times 10^{-11}$

time delay between their flashes should be considered for in-line estimation of carrier dynamics in 3D perovskite films for photovoltaics.

4. Discussion

This work demonstrates that monitoring the TIPL after a double-pulse excitation in which the separation between the two pulses can be controllably swept is a facile, precise, and accurate method for establishing the dynamics of excitons, free charge carriers, or even a mixture of both in perovskite materials. We employed quasi-2D perovskites and a 3D perovskite to demonstrate this.

We found in our previous work that the ASE threshold of quasi-2D perovskites decreases when the bimolecular free carrier emission increases.[33] As the excitation fluence increases the initial PL emission of free carriers increases with the square of the fluence while at high fluences the emission lifetime decreases. This leads to a high initial photon density which allows ASE to occur. Quasi-2D perovskites have led to promising results in the field of lasing.[40,41] Understanding the bimolecular rate constant of the used materials is an important task for the further development of these materials, and the presented double-excitation method could be of use in this respect to groups where access to tools such as streak cameras are limited.

The potential of this technology for the characterization of PV materials is even more relevant. Determining the free charge carrier recombination pathways and rates in the active layer of PV devices can reveal material quality during the cell fabrication process. Correlating this with ultimate device performance, the recombination dynamics measured after the formation of the perovskite active layer (before the deposition of capping charge transport layers and/or top electrode) can be useful to provide quality control and feedback to the process parameters. In terms of measuring the carrier dynamics, the two-pulse method has attractive features in comparison to a method based on a streak camera or time-correlated single photon counting in terms of simplicity and expense of the equipment required, but also in terms of the potential to image the carrier dynamics across the whole area of the sample.

In terms of equipment simplicity and cost, this technique needs two pulses that are short compared to the excited-state lifetime of the sample and arrive with a controllable delay between them. Synchronizing an actively Q-switched laser to a passively Q-switched laser through a delay generator would be a robust and cost-effective solution to generate such a pulse sequence. The PL generated could then be captured by a simple USB spectrometer, like in this paper. On the other hand, if the beam size of the pulses is expanded to cover a larger area of the sample, the carrier dynamics could be imaged over this test area by using an industrial camera to capture the steady-state PL. In this case, the change in the PL intensity with delay time at each spatial location (camera pixel, or group of camera pixels) could be independently analyzed to indicate how spatially uniform the carrier dynamics are. For photovoltaic films in which only low fluences are necessary to observe changes in the relative PLQY for samples dominated by free charge carriers, it should also be possible to use LEDs to excite the samples, as discussed above.

To do this on a larger area, some development work needs to be done developing arrays of synchronously firing LEDs to provide reasonably uniform illumination over the whole sample area (likely actually an interweaving of two separate arrays each pulsing in unison but with a time delay between them). The possible advantages of this technology in terms of cost, speed, and robust implementation of carrier-dynamic measurements, and the potential to image these, make this an attractive method to further test and develop.

In terms of practical application, the time required to make these measurements is an important aspect. In the work presented herein, each measurement consists of 120 measured delay points with each point being exposed to the laser pulse trains for 0.8 s with a background correction of an additional 0.8 s leading to a total measurement time of slightly over 3 min for complete measurement of the relative PLQY as a function of delay time for a single excitation fluence. The relative PLQY is measured by observing the changes in the PL emission and no PLQY measurement involving an integrating sphere is necessary. As the carrier recombination coefficients can be uniquely extracted from a curve at a single fluence, measurement at a single fluence is sufficient for a rough estimate of the recombination coefficients. We note that as a rule of thumb, this fluence should be chosen (either through prior knowledge of similar systems or by some initial trial and error) such that the monomolecular and bimolecular decay rates are equal at the excited-state density reached when both pulses overlap. Thus, the current method is favorable in terms of the time taken to measure a single fluence as the more traditional methods involving time-resolved detection of the PL. Further improvements in the time required to take the measurements could be achieved by investigating faster repetition rates and shorter integration times on the camera, and/or taking fewer time delays and fitting a more sparsely populated curve. In comparison with TRPL techniques that give full time resolution of the excited-state evolution, the more limited information obtained from this time-integrated double-pulse method will never provide as nuanced information on the excited-state dynamics. Thus, to check advanced models in detail, for example, models that might take into account time dependencies of the recombination coefficients, laboratory techniques such as Streak Camera measurements or TCSPC remain favorable. However, for a rough estimate of the excited-state dynamics with a robust and low-cost system (desirable for example in scalable quality control of perovskite photovoltaic layers), we see distinct advantages and opportunities for further development of the double pulse method.

5. Conclusion

In this work, we consider a characterization method to extract the rate constants from the TIPL of different perovskite materials based on the excitation with two laser pulses with a variable temporal delay and the measurement of the relative PLQY changes. We find that the relative PLQY is higher for free carrier dominated PL and decreases with temporal delay and the relative PLQY for excitonic PL is lower and increases with temporal delay. We analyze the TIPL of quasi-2D perovskites based on the BA and NMA spacer molecules at different

concentrations to show the different relative PLQY-curves depending on the dominance of excitons, free charge carriers, or a mixture of both. We find that the extracted parameters are like the ones we determined in a previous work based on TRPL measurements of the same type of perovskites. We further demonstrate the significance of this method for the characterization of photovoltaic materials by considering an unpassivated and a passivated 3D perovskite. We conclude that the simple rate constants of several types of perovskites can be extracted with the double pulse method, and suggest that it is attractive for developing "in-line" basic characterization of excited-state lifetimes, especially in perovskite solar cell layers.

6. Experimental Section

Perovskite Fabrication: The perovskite films in this work were produced by dissolving 239.1 mg of $CsPbBr_3$ in 1 mL of DMSO, then heating the solution for about 20 min at 60 °C. The solution was then admixed with either BABr/DMSO (2.8 m) or NMABr/DMSO (2.8 m) to reach the desired elemental composition $CsPbBr_3(BABr)_\gamma$ where γ is the molar fraction (0.4 and 1.0 in this work). The resulting solution was spin-coated on glass substrates in a two-step process at 1000 rpm (ramp rate: 1000 rpm s^{-1}) for 20 s and then 4000 rpm (ramp rate: 1000 rpm s^{-1}) for 40 s. Finally, the films were annealed at 70 °C for 10 min. The unpassivated 3D perovskite was made following the instructions described by Prochowicz et al.[42] For the passivated perovskite we followed the method described by Gharibzadeh et al.[37]

Characterization: For the excitation, we used a femtosecond laser in combination with an optical parametric amplifier (Light Conversion, Pharos/Orpheus, 260 fs) to get a wavelength of 430 nm at a repetition rate of either 1 kHz for the NMA samples or 100 Hz for the BA samples. The spot size was 2.5×10^{-2} cm^2. The PL emission was collimated with a lens with a 5 cm focal length and into the fiber of a spectrometer (QEPro, Ocean Optics). For the delay, we used a retroreflector mounted on a linear translation stage that can cover 60 cm which equates to a delay time of up to 4 ns. For the characterization of the 3D perovskite, an additional Q-switched laser (InnoLas, picolo MOPA, 600 ps) was used at a repetition rate of 1 kHz at a wavelength of 532 nm which was combined with the aforementioned LightConversion system set at the same wavelength. For the delay between the laser pulses, a delay generator (DG535, Stanford Research Systems) was used. The spot size was 3.5×10^{-2} cm^2. For the TRPL a streak camera (Hamamatsu Universal C10910) combined with a spectrometer (Acton SpectraProSP2300) was used.

Statistical Analysis: For the experimental data shown in Figures 4, 5, and 7, the data are fit for each fluence/measurement using Origin (OriginLab) with the extracted parameters being the mean values of the results. The uncertainties are determined from the statistical evaluation of the fitting parameters. For data considering both excitons and free carriers, a global fit is used instead whereby the fitting parameters are shared over different excitation fluences. Least square regression is used to fit the data. The Levenberg–Marquardt algorithm is used to fit and determine the errors of the global fits. For the TRPL data statistical weights are used in the fitting process ($1/y_i$). The "relative PLQY" data are prepared by dividing the integrated photoluminescence of a sample with double pulse excitation with the integrated photoluminescence of a single pulse excitation (all excitation pulses contain the same energy). Each measurement was done on a single respective sample. For the quantitative comparison of fits considering either just one excited-state species or both the reduced χ^2 value in combination with global fitting is used.

Supporting Information

Supporting Information is available from the Wiley Online Library or from the author.

Conflict of Interest

The authors declare no conflict of interest.

Data Availability Statement

The data that support the findings of this study are available from the corresponding author upon reasonable request.

[1] N. Wang, L. Cheng, R. Ge, S. Zhang, Y. Miao, W. Zou, C. Yi, Y. Sun, Y. Cao, R. Yang, Y. Wei, Q. Guo, Y. Ke, M. Yu, Y. Jin, Y. Liu, Q. Ding, D. Di, L. Yang, G. Xing, H. Tian, C. Jin, F. Gao, R. H. Friend, J. Wang, W. Huang, *Nat. Photonics* **2016**, *10*, 699.

[2] L. Cheng, T. Jiang, Y. Cao, C. Yi, N. Wang, W. Huang, J. Wang, *Adv. Mater.* **2020**, *32*, 1904163.

[3] J. Byun, H. Cho, C. Wolf, M. Jang, A. Sadhanala, R. H. Friend, H. Yang, T.-W. Lee, *Adv. Mater.* **2016**, *28*, 7515.

[4] Z. Ren, J. Yu, Z. Qin, J. Wang, J. Sun, C. C. S. Chan, S. Ding, K. Wang, R. Chen, K. S. Wong, X. Lu, W.-J. Yin, W. C. H. Choy, *Adv. Mater.* **2021**, *33*, 2005570.

[5] Y. Jiang, J. Wei, M. Yuan, *J. Phys. Chem. Lett.* **2021**, *12*, 2593.

[6] W. Bi, Q. Cui, P. Jia, X. Huang, Y. Zhong, D. Wu, Y. Tang, S. Shen, Y. Hu, Z. Lou, F. Teng, X. Liu, Y. Hou, *ACS Appl. Mater. Interfaces* **2020**, *12*, 1721.

[7] Y. Han, S. Park, C. Kim, M. Lee, I. Hwang, *Nanoscale* **2019**, *11*, 3546.

[8] X. Yang, X. Zhang, J. Deng, Z. Chu, Q. Jiang, J. Meng, P. Wang, L. Zhang, Z. Yin, J. You, *Nat. Commun.* **2018**, *9*, 570.

[9] B. Zhao, S. Bai, V. Kim, R. Lamboll, R. Shivanna, F. Auras, J. M. Richter, L. Yang, L. Dai, M. Alsari, X.-J. She, L. Liang, J. Zhang, S. Lilliu, P. Gao, H. J. Snaith, J. Wang, N. C. Greenham, R. H. Friend, D. Di, *Nat. Photonics* **2018**, *12*, 783.

[10] M. Ban, Y. Zou, J. P. H. Rivett, Y. Yang, T. H. Thomas, Y. Tan, T. Song, X. Gao, D. Credgington, F. Deschler, H. Sirringhaus, B. Sun, *Nat. Commun.* **2018**, *9*, 3892,

[11] Y. Miao, L. Cheng, W. Zou, L. Gu, J. Zhang, Q. Guo, Q. Peng, M. Xu, Y. He, S. Zhang, Y. Cao, R. Li, N. Wang, W. Huang, J. Wang, *Light, Sci. Appl.* **2020**, *9*, 89.

[12] J. Calabrese, N. L. Jones, R. L. Harlow, N. Herron, D. L. Thorn, Y. Wang, *J. Am. Chem. Soc.* **1991**, *113*, 2328.

[13] P. Tyagi, S. M. Arveson, W. A. Tisdale, *J. Phys. Chem. Lett.* **2015**, *6*, 1911.

[14] L. Cheng, Y. Cao, R. Ge, Y.-Q. Wei, N.-N. Wang, J.-P. Wang, W. Huang, *Chin. Chem. Lett.* **2017**, *28*, 29.

[15] L. N. Quan, M. Yuan, R. Comin, O. Voznyy, E. M. Beauregard, S. Hoogland, A. Buin, A. R. Kirmani, K. Zhao, A. Amassian, D. H. Kim, E. H. Sargent, *J. Am. Chem. Soc.* **2016**, *138*, 2649.

[16] X. Hong, T. Ishihara, A. V. Nurmikko, *Phys. Rev. B* **1992**, *45*, 6961.

[17] T. Ishihara, *J. Lumin.* **1994**, *60–61*, 269.

[18] J. C. Blancon, A. V. Stier, H. Tsai, W. Nie, C. C. Stoumpos, B. Traoré, L. Pedesseau, M. Kepenekian, F. Katsutani, G. T. Noe, J. Kono, S. Tretiak, S. A. Crooker, C. Katan, M. G. Kanatzidis, J. J. Crochet, J. Even, A. D. Mohite, *Nat. Commun.* **2018**, *9*, 2254.

[19] C. C. Stoumpos, D. H. Cao, D. J. Clark, J. Young, J. M. Rondinelli, J. I. Jang, J. T. Hupp, M. G. Kanatzidis, *Chem. Mater.* **2016**, *28*, 2852.

[20] J. Cho, J. T. DuBose, P. V. Kamat, *J. Phys. Chem. Lett.* **2020**, *11*, 2570.

[21] C. L. Davies, M. R. Filip, J. B. Patel, T. W. Crothers, C. Verdi, A. D. Wright, R. L. Milot, F. Giustino, M. B. Johnston, L. M. Herz, *Nat. Commun.* **2018**, *9*, 293.

[22] M. Yuan, L. N. Quan, R. Comin, G. Walters, R. Sabatini, O. Voznyy, S. Hoogland, Y. Zhao, E. M. Beauregard, P. Kanjanaboos, Z. Lu, D. H. Kim, E. H. Sargent, *Nat. Nanotechnol.* **2016**, *11*, 872.

[23] L. Lei, D. Seyitliyev, S. Stuard, J. Mendes, Q. Dong, X. Fu, Y.-A. Chen, S. He, X. Yi, L. Zhu, C.-H. Chang, H. Ade, K. Gundogdu, F. So, *Adv. Mater.* **2020**, *32*, 1906571.

[24] D. Ma, K. Lin, Y. Dong, H. Choubisa, A. H. Proppe, D. Wu, Y.-K. Wang, B. Chen, P. Li, J. Z. Fan, F. Yuan, A. Johnston, Y. Liu, Y. Kang, Z.-H. Lu, Z. Wei, E. H. Sargent, *Nature* **2021**, *599*, 594.

[25] L. Kong, X. Zhang, Y. Li, H. Wang, Y. Jiang, S. Wang, M. You, C. Zhang, T. Zhang, S. V. Kershaw, W. Zheng, Y. Yang, Q. Lin, M. Yuan, A. L. Rogach, X. Yang, *Nat. Commun.* **2021**, *12*, 1246.

[26] M. Kaiser, Y. Li, I. Allegro, B. S. Richards, U. W. Paetzold, I. A. Howard, *Adv. Mater. Interfaces* **2021**, *8*, 2101326.

[27] V. Gulbinas, R. Jakubenas, S. Pakalnis, A. Undzenas, *J. Chem. Phys.* **1997**, *107*, 4927.

[28] C. H. Lui, K. F. Mak, J. Shan, T. F. Heinz, *Phys. Rev. Lett.* **2010**, *105*, 127404.

[29] D. Sun, G. Aivazian, A. M. Jones, J. S. Ross, W. Yao, D. Cobden, X. Xu, *Nat. Nanotechnol.* **2012**, *7*, 114.

[30] R. Röder, T. P. H. Sidiropoulos, C. Tessarek, S. Christiansen, R. F. Oulton, C. Ronning, *Nano Lett.* **2015**, *15*, 4637.

[31] V. Sarritzu, N. Sestu, D. Marongiu, X. Chang, Q. Wang, M. A. Loi, F. Quochi, M. Saba, A. Mura, G. Bongiovanni, *Adv. Opt. Mater.* **2018**, *6*, 1700839.

[32] W. Wang, Y. Li, X. Wang, Y. Lv, S. Wang, K. Wang, Y. Shi, L. Xiao, Z. Chen, Q. Gong, *Phys. Rev. B* **2016**, *94*, 140302.

[33] Y. Li, I. Allegro, M. Kaiser, A. J. Malla, B. S. Richards, U. Lemmer, U. W. Paetzold, I. A. Howard, *Mater. Today* **2021**, *49*, 35.

[34] M. J. Simpson, B. Doughty, B. Yang, K. Xiao, Y.-Z. Ma, *J. Phys. Chem. Lett.* **2015**, *6*, 3041.

[35] S. Yu, Y. Yan, M. Abdellah, T. Pullerits, K. Zheng, Z. Liang, *Small* **2019**, *15*, 1905081.

[36] A. Kiligaridis, P. A. Frantsuzov, A. Yangui, S. Seth, J. Li, Q. An, Y. Vaynzof, I. G. Scheblykin, *Nat. Commun.* **2021**, *12*, 3329.

[37] S. Gharibzadeh, P. Fassl, I. M. Hossain, P. Rohrbeck, M. Frericks, M. Schmidt, T. Duong, M. R. Khan, T. Abzieher, B. A. Nejand, F. Schackmar, O. Almora, T. Feeney, R. Singh, D. Fuchs, U. Lemmer, J. P. Hofmann, S. A. L. Weber, U. W. Paetzold, *Energy Environ. Sci.* **2021**, *14*, 5875.

[38] A. Kaukher, *LED Pulser: A Light-Emitting Diode–Based Light Source for 2D Detectors*, European X-Ray Free-Electron Laser Facility GmbH, Germany **2017**.

[39] N. B. Hassan, F. Dehkhoda, E. Xie, J. Herrnsdorf, M. J. Strain, R. Henderson, M. D. Dawson, **2021**, https://doi.org/10.48550/arXiv.2111.13586.

[40] C. Qin, A. S. D. Sandanayaka, C. Zhao, T. Matsushima, D. Zhang, T. Fujihara, C. Adachi, *Nature* **2020**, *585*, 53.

[41] M. R. Leyden, S. Terakawa, T. Matsushima, S. Ruan, K. Goushi, M. Auffray, A. S. D. Sandanayaka, C. Qin, F. Bencheikh, C. Adachi, *ACS Photonics* **2019**, *6*, 460.

[42] D. Prochowicz, R. Runjhun, M. M. Tavakoli, P. Yadav, M. Saski, A. Q. Alanazi, D. J. Kubicki, Z. Kaszkur, S. M. Zakeeruddin, J. Lewiński, M. Grätzel, *Chem. Mater.* **2019**, *31*, 1620.